Journal of Power Sources 196 (2011) 2602–2607

Contents lists available at ScienceDirect

Journal of Power Sources

journal homepage: www.elsevier.com/locate/jpowsour

Electrochemical performance of $BaZr_{0.1}Ce_{0.7}Y_{0.1}Yb_{0.1}O_{3-\delta}$ electrolyte based proton-conducting SOFC solid oxide fuel cell with layered perovskite $PrBaCo_2O_{5+\delta}$ cathode

Hanping Ding, Yuanyuan Xie, Xingjian Xue *

Department of Mechanical Engineering, University of South Carolina, Columbia, SC 29208, USA

ARTICLE INFO

Article history:
Received 16 September 2010
Received in revised form 23 October 2010
Accepted 26 October 2010
Available online 3 November 2010

Keywords:
Solid oxide fuel cells
Layered perovskite
Polarization resistance
Cathode

ABSTRACT

$BaZr_{0.1}Ce_{0.7}Y_{0.1}Yb_{0.1}O_{3-\delta}$ (BZCYYb) exhibits adequate protonic conductivity as well as sufficient chemical and thermal stability over a wide range of SOFC operating conditions, while layered perovskite $PrBaCo_2O_{5+\delta}$ (PBCO) has advanced electrochemical properties. This research fully takes advantage of these advanced properties and develops a novel protonic ceramic membrane fuel cell (PCMFC) of Ni–BZCYYb|BZCYYb|PBCO. The performance of the button cell was tested under intermediate-temperature range from 600 to 700 °C with humified H_2 (~3% H_2O) as fuel and ambient air as oxidant. The results show that the open circuit potential of 0.983 V and the maximal power density of 490 mW cm^{-2} were achieved at 700 °C. By co-doping barium zirconate–cerate with Y and Yb, the conductivity of electrolyte was significantly improved. The polarization processes of the button cell were characterized using the complicated electrochemical impedance spectroscopy technique. The results indicate that the polarization resistances contributed from both charge migration processes and mass transfer processes increase with decreasing cell voltage loads. However the polarization resistance induced by mass transfer processes is negligible in the studied button cell.

1. Introduction

Solid oxide electrolytes utilized in traditional solid oxide fuel cells are oxygen ionic conductors [1], typically including high temperature electrolyte yttria stabilized zirconia (YSZ), and intermediate temperature doped ceria-based electrolytes. In ionic conducting electrolyte based SOFC, ions are generated at cathode electrode through oxygen reduction reactions, and migrate from cathode side to anode side. Proton conductors are relatively new electrolytes employed in recent SOFC development [2,3], and show great advantages over oxide-ion conducting ones, such as low activation energy [4] and high energy efficiency [5]. The state-of-the-art proton conducting materials are barium-based perovskite-type oxides, e.g., $BaCeO_{3-\delta}$ and $BaZrO_{3-\delta}$. By suitable doping, these materials may obtain both adequate proton conductivity as well as sufficient chemical and thermal stability over a wide range of SOFC operating conditions [6]. Recent progress shows that $BaZr_{0.1}Ce_{0.7}Y_{0.1}Yb_{0.1}O_{3-\delta}$ (BZCYYb) [7] may obtain high conductivity in lower temperature conditions. Nevertheless, BZCYYb electrolyte based SOFC studies are still at early stages in open literatures.

It is generally recognized that the cathode is the cell component limiting the electrochemical performance of anode-supported SOFCs. One of the fundamental requirements for SOFC cathode material is a high oxygen reduction rate. The reduction reaction is strictly confined to triple phase boundary (TPB) sites, where the oxygen molecules combine with electrons and form into ions. The mixed ionic and electronic conductors (MIEC) may potentially extend TPB active region over the entire cathode. In this respect, many simple perovskite-type MIEC such as doped $LaCoO_3$ [8], $BaCoO_3$ [9] and $SmCoO_3$ [10] have been extensively studied as cathode candidates for SOFCs. Recently layered perovskite oxide $PrBaCo_2O_{5+\delta}$ (PBCO) with ordered A-cations has also been investigated as potential cathode material by Kim et al. [11–13]. This compound can be theoretically described with the stacking sequence of, e.g., ...|BaO|CoO_2|PrO_x|CoO_2.... When $x < 1$, the ordered A-cations localizing oxygen vacancies appear within the rare earth layers [14,15]. This characteristic has a great potential to improve cathode performance. When a simple cubic perovskite with randomly occupied A-sites transfers into a layered crystal structure with ordered lanthanide and alkali-earth layers, it reduces the strength of oxygen binding and provides disorder-free channels for ionic migration.

In our previous work, $PrBa_{0.5}Sr_{0.5}Co_2O_{5+\delta}$ and $GdBa_{0.5}Sr_{0.5}Co_2O_{5+\delta}$ layered perovskite oxides have been investigated and shown promising electrochemical properties in button

* Corresponding author. Tel.: +1 803 576 5598; fax: +1 803 777 0106.
E-mail address: Xue@cec.sc.edu (X. Xue).

0378-7753/$ – see front matter © 2010 Elsevier B.V. All rights reserved.
doi:10.1016/j.jpowsour.2010.10.069

cell tests, e.g., the maximal power densities of NiO–SDC/SDC (~20 μm)/$PrBa_{0.5}Sr_{0.5}Co_2O_{5+\delta}$ button cell and Ni–$BaZr_{0.1}Ce_{0.7}Y_{0.2}O_{3-\delta}$/$BaZr_{0.1}Ce_{0.7}Y_{0.2}O_{3-\delta}$ (~20 μm)/$GdBa_{0.5}Sr_{0.5}Co_2O_{5+\delta}$ can reach 1045 and 430 mW cm^{-2} at 700 °C, respectively, while the electrode polarization resistances are 0.05 and 0.08 Ω cm^2, respectively, at 700 °C [2,16]. However, the electrochemical performance of layered perovskite cathode material based on BZCYYb electrolyte is not reported yet in open literatures. In this study, the performance of a layered perovskite PBCO cathode on BZCYYb electrolyte is investigated under intermediate temperature conditions. Particularly, the conductivity and activity energy are characterized for PBCO cathode material. The polarization performance of the button cell NiO–BZCYYb/BZCYYb/PBCO is tested. The electrochemical performance of the cell is systematically characterized using complex impedance technique under different cell load conditions.

2. Experimental

2.1. Sample preparation, cell fabrication, and X-ray diffraction measurement

The $BaZr_{0.1}Ce_{0.7}Y_{0.1}Yb_{0.1}O_{3-\delta}$ (BZCYYb) powders were synthesized using modified Pechini method, where citrate and ethylenediamine tetraacetic acid (EDTA) were employed as parallel complexing agents. Y_2O_3 and Yb_2O_3 was first dissolved in nitric acid under heating; the calculated amount of $Ba(NO_3)_2{\cdot}9H_2O$, $Ce(NO_3)_3{\cdot}6H_2O$ and $Zr(NO_3)_4{\cdot}4H_2O$ was dissolved in EDTA–NH_3 aqueous solution. After agitation for a certain time, a proper amount of citric acid was introduced, the molar ratio of EDTA:citric acid:total of metal cations was controlled around 1:1.5:1. After converted into viscous gel under heating and stirring conditions, the solution ignited to flame and resulted in ash. The resulting ash-like material was afterwards calcined at 1100 °C for 5 h in air to form a pure perovskite oxide, and the synthesized BZCYYb powders were then obtained.

The anode-supported BZCYYb bi-layer (Φ = 15 mm) was prepared by a dry-pressing method. The mixture of NiO + BZCYYb + starch (60%:40%:20% in weight) was pre-pressed at 200 MPa and formed into an anode substrate. The anode functional layer (mixture of NiO and BZCYYb, NiO: BZCYYb = 60%:40% in weight) was then pressed onto the substrate. Then loose BZCYYb powder synthesized above was uniformly distributed onto the anode substrate, co-pressed at 250 MPa, and subsequently co-sintered at 1400 °C for 5 h to obtain bi-layer anode electrode/electrolyte assembly.

Layered $PrBaCo_2O_{5+\delta}$ (PBCO) powder was synthesized using Pechini process with Pr_6O_{11}, $Ba(NO_3)_2{\cdot}9H_2O$ and $Co(NO_3)_2{\cdot}6H_2O$ as precursors, followed by calcinations at 950 °C for 5 h. Fine PBCO powders were then mixed thoroughly with a Heraeus binder (V-006) to prepare the cathode slurry. The slurry was painted on BZCYYb electrolyte films, which was then sintered at 950 °C for 3 h in air to form single cells of NiO–BZCYYb/BZCYYb/PBCO.

The phase identification of the prepared cathode and electrolyte powders were studied with the powder X-ray diffraction by Cu-Kα radiation (D/MAX-3C).

2.2. Electrochemical characterization

The electrical conductivity of PBCO in air was measured from 200 °C to 800 °C using a standard DC four-probe technique on a H.P. multimeter (Model 34401A). Single cells were tested from 600 to 700 °C with humidified hydrogen (~3% H_2O) as fuel and the static air as oxidant. The flow rate of fuel was controlled at 30 ml min^{-1} using a precision flow meter (APEX). The voltage–current curves were recorded by DC load (BK-8500) at the scanning rate of 30 mV s^{-1}. The electrochemical impedance spectra (EIS) were obtained using a Solatron 1260 frequency response analyzer in combination with a Solartron 1287 potentiostat over the frequency range from 0.01 Hz to 10^5 Hz under open circuit conditions as well as different loading conditions. A scanning electron microscope (SEM, FEI Quanta 200) was used to observe the microstructure of the sintered PBCO rectangular sample and the post-test cell.

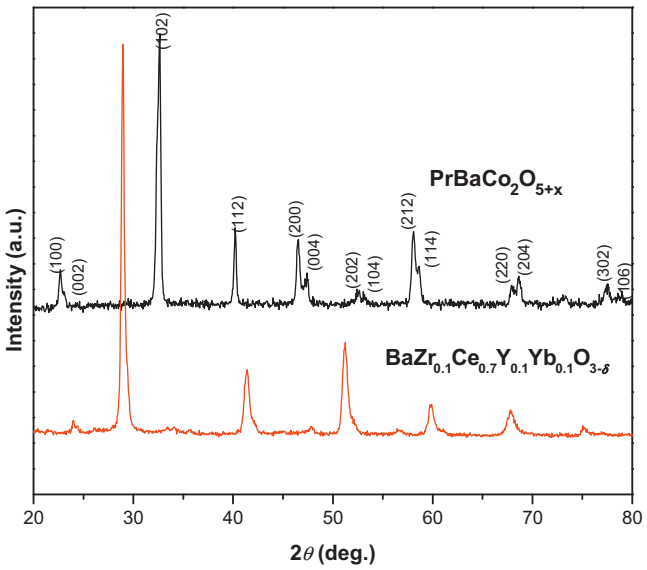

Fig. 1. XRD patterns for (a) the layered $PrBaCo_2O_{5+\delta}$ (PBCO) cathode powders, (b) BZCYYb electrolyte powders.

3. Results and discussion

As shown in Fig. 1(a), the as-prepared powder of PBCO exhibits a pure layered perovskite phase with orthorhombic lattice geometry of space group (*Pmmm*) which is consistent with that reported by Kim et al. [17]. The cell parameters of PBCO obtained using software unit cell are: a = 3.9041 Å, b = 3.8336 Å, c = 7.6817 Å, V = 114.94 $Å^3$. Fig. 1(b) also presents the diffraction patterns of BZCYYb electrolyte sintered at 1400 °C for 5 h. It can be clearly seen that there are only peaks corresponding to the cubic perovskite phase [3]. The co-doping of Y and Yb into $BaZr_{0.1}Ce_{0.9}O_{3-\delta}$ does not change the phase structure.

The total conductivity of PBCO in air was obtained using a four-probe DC technique (Fig. 2(a)). It can be seen that the conductivity rapidly decreases from 1980 to 255 S cm^{-1} with increasing the temperature from 200 to 500 °C, and then gradually decreases to 97 S cm^{-1} at 800 °C. This result indicates that the conductivity of PBCO is metal-like behavior [18]. Zhang et al. reported that the transition of insulator–metal behavior occurred about 150 °C [18]. In general, the required conductivity for cathode materials is 10^2 S cm^{-1} or above [19]. Therefore PBCO is a good cathode material in terms of conductivity. Since the ionic conductivity is much lower than the electronic conductivity, the data obtained here is believed to be dominated by the electronic conductivity. Shown in Fig. 2(c) is the SEM of the surface of the rectangular sample. The sample is close to 100% dense, consequently the conductivity obtained here can be treated as intrinsic conductivity of PBCO. It is believed that the electronic conduction of PBCO occurs through electron hopping along Co–O–Co bonds [18]. When the operating temperature increases, the oxygen vacancies will increase. The creation of oxygen vacancies will break the Co–O–Co bonds. As a result, the electronic conductivity of PBCO decreases with increasing temperatures.

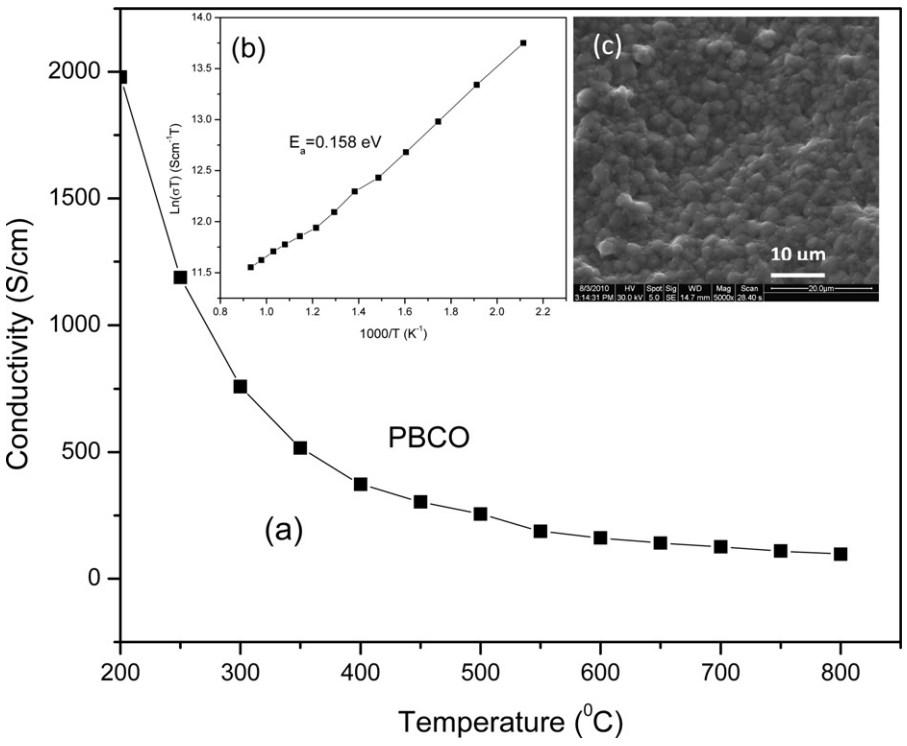

Fig. 2. Temperature dependence of electrical conductivity of PBCO (a) at 200–800 °C in air; (b) with $\ln(\sigma T)$ versus $1000T^{-1}$; (c) surface view of sintered rectangular sample.

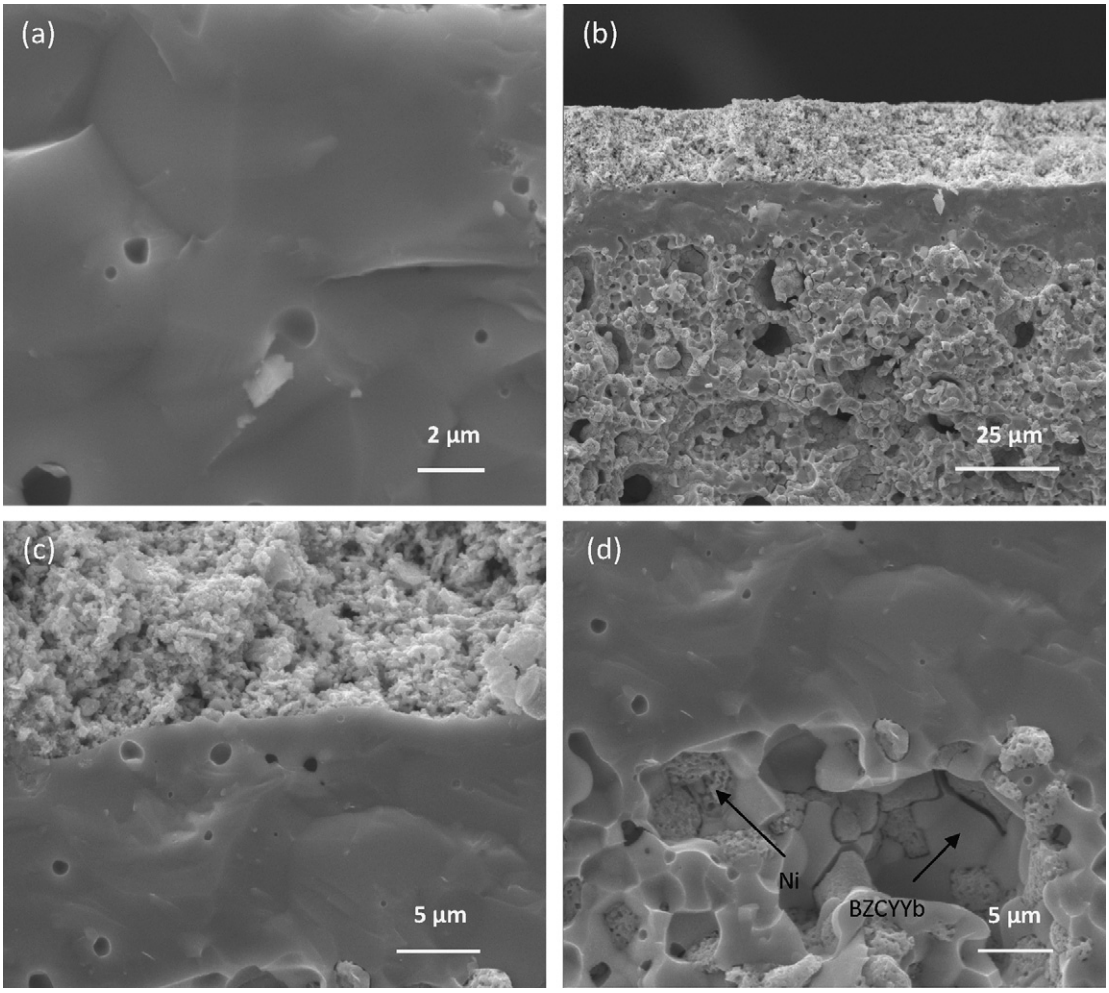

Fig. 3. SEM micrographs of cell after testing: (a) surface of electrolyte; (b) the cross-section with a 15 μm-thick BZCYYb membrane; (c) interface of cathode and electrolyte; (d) interface of electrolyte and anode.

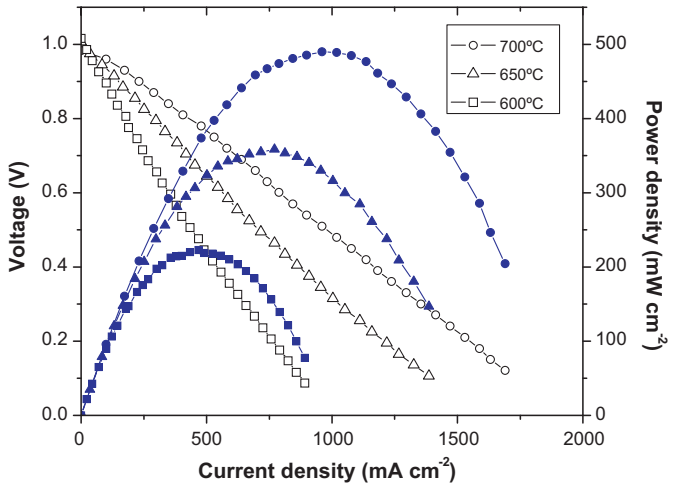

Fig. 4. Performance of the as-prepared cell with hydrogen at different temperatures.

The measured conductivity data of PBCO is employed to determine its activation energy according to the Arrhenius equation,

$$\sigma = \frac{A}{T}\exp\left(-\frac{E_a}{kT}\right) \quad (1)$$

where σ is the electronic conductivity, A is the pre-exponential factor, T is the absolute temperature, k is Boltzmann constant, and E_a is the activation energy.

Shown in Fig. 2(b) is the linear relationship between $\ln(\sigma T)$ and $1/T$ obtained from electronic conductivity data. The activation energy E_a of PBCO obtained from Fig. 2(b) is about 0.158 eV.

After electrochemical test, the cross-sectional view of as-prepared tri-layer cell and the surface of electrolyte are examined using SEM. One can see from Fig. 3(a) that the BZCYYb electrolyte membrane is dense, no pores or cracks can be observed. The thickness of fabricated electrolyte is about 15 μm, and that of PBCO cathode layer is about 25 μm (Fig. 3(b)). The cathode layer adheres to the electrolyte layer fairly well (Fig. 3(c)). The uniformly distributed micropores in the cathode layer can greatly facilitate the oxygen diffusion and reduction reactions. In the anode substrate (Fig. 3(d)), BZCYYb grains form the network inter-penetrating with nickel particle network, providing material backbone for protons and electrons migration.

The electrochemical performance of the as-prepared cell is experimentally obtained and shown in Fig. 4 under different operating temperatures, including I–V curves and I–P curves. In general, the open-circuit voltage (OCV) of the cell should be close to its theoretic value of 1.1 V [20], and is slightly influenced by operating conditions. Two factors lead to the fact that the practical OCV is usually lower than its theoretical value. One is that a slight electron current might exist through electrolyte membrane, which is regarded as current leakage; the higher the current leakage exists, the lower the cell OCV will be. Another factor is that fuel/gas cross flow might take place when electrolyte membrane is not dense, causing lower OCV value as well. The OCVs shown in Fig. 4 are 0.983 V at 700 °C, 1.007 V at 650 °C, 1.016 V at 600 °C, indicating that the voltage drop caused by current leakage and fuel/gas cross flow is negligible. Further study is needed to identify these two contributions individually in the future. Results in Fig. 4 also show that the peak power densities are 490, 358 and 223 mW cm^{-2} at 700, 650 and 600 °C, respectively. Compared with other proton-conducting single cell with PBCO cathode (anode supported Ni–$BaZr_{0.1}Ce_{0.7}Y_{0.1}O_{3-\delta}$ (BZCY7)/BZCY7/$PrBaCo_2O_{5+\delta}$), the output is higher at the same temperatures (349 and 183 mW cm^{-2}) [21]. Liu et al. [7] demonstrated that BZCYYb displayed the highest conductivity below 750 °C compared with that of several other SOFC electrolyte materials, such as YSZ, GDC and BZCY7. The high cell performance observed in the experiments is partially due to the high electrolyte conductivity of barium zirconate–cerate co-doped with Y and Yb. This will be elaborated as follows.

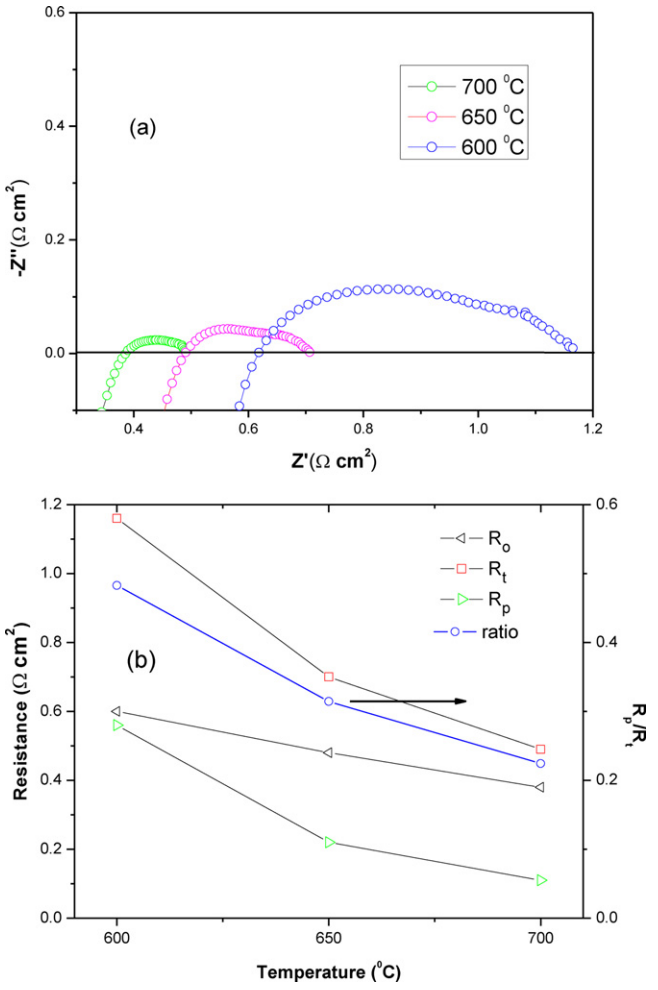

Fig. 5. (a) Impedance spectra and (b) the electrode polarization resistances, electrolyte resistances, and total resistances determined from the impedance spectra of the as-prepared cell measured under open-circuit conditions at different temperatures. R_p/R_t is also shown in (b).

The polarization processes of Ni–BZCYYb/BZCYYb/PBCO cells are examined using electrochemical impedance spectra (EIS). The impedance spectra of the as-prepared cells are first measured under open-circuit conditions at different temperatures, and are shown in Fig. 5(a). In these spectra, three parameters can be directly determined. The cell total resistance (R_t) is the spectra interception with real-axis at low frequency; the cell ohmic resistance (R_o) is the spectra interception with real-axis at high frequency; the polarization resistance (R_p) is the difference between R_t and R_o. The values determined from the impedance spectra in Fig. 5(a) are shown in Fig. 5(b). One can see that R_p is significantly reduced with increasing temperatures, typically from 0.56 Ω cm^2 at 600 °C to 0.11 Ω cm^2 at 700 °C, respectively. The R_p values are well comparable to those of similar proton conducting cells with other layered perovskite cathodes, such as $GdBaCo_2O_{5+\delta}$ [22] (0.16 Ω cm^2 at 700 °C).

As shown in Fig. 5(b), the cell resistance contributed from electrode polarization is lower than that from R_o, particularly at high temperature conditions. The ratio of R_p to R_t decreases with increasing the operating temperatures, from 48.2% at 600 °C to 22.4% at 700 °C, respectively. By co-doping barium zirconate–cerate with

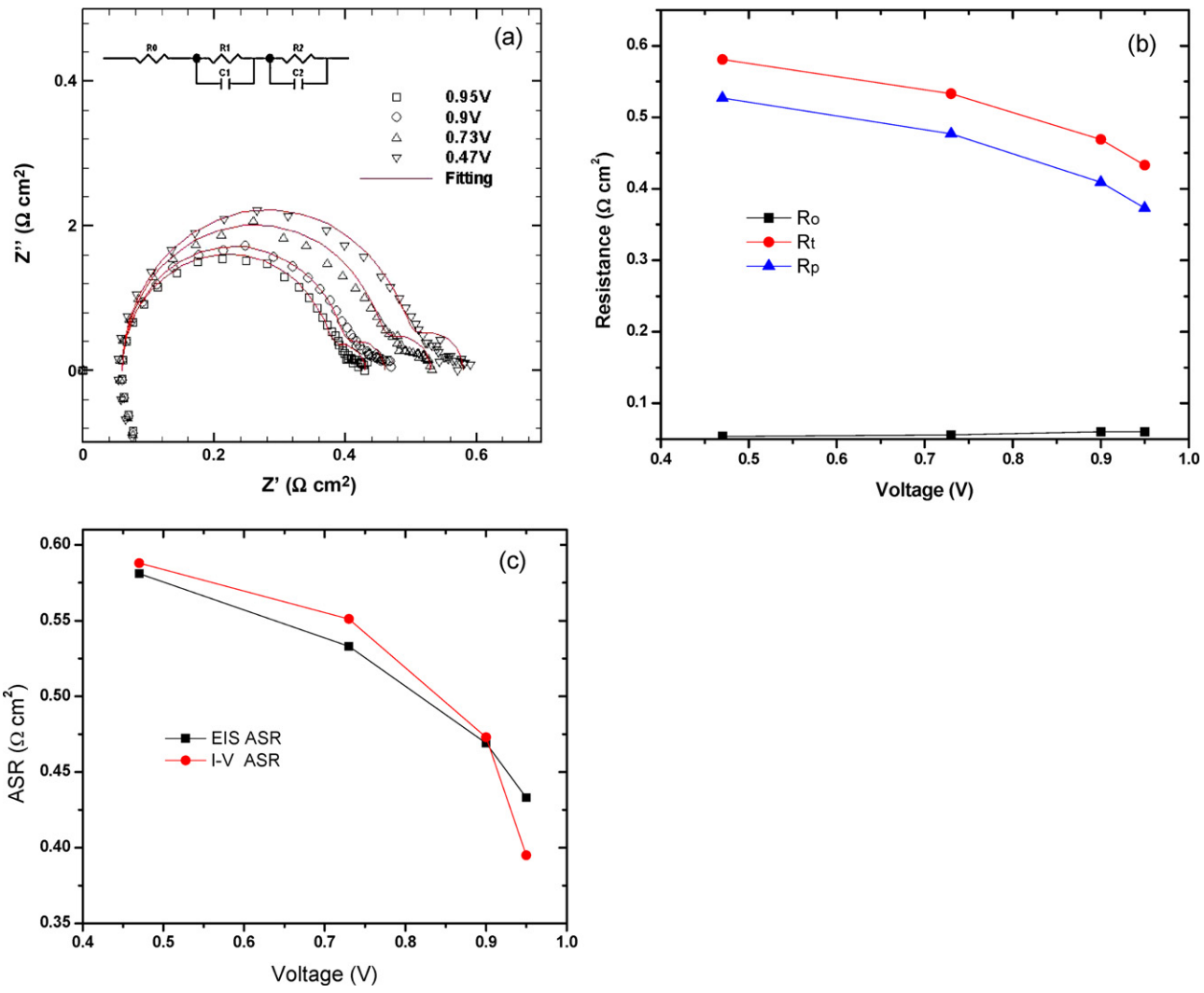

Fig. 6. (a) Impedance spectra of the cell at 700 °C under different voltage conditions; (b) the corresponding total cell resistance (R_t), ohmic resistance (R_o), as well as polarization resistance (R_p) and (c) ASR values comparison by EIS and *I–V* curve at 700 °C.

elements Y and Yb, the conductivity of electrolyte was significantly improved. The ohmic resistance of the single cell is 0.38 Ω cm^2 at 700 °C as shown in Fig. 5(b), in which the BZCYYb electrolyte thickness is about 15 μm as shown in Fig. 2. As a comparison, the ohmic resistance of the cell in [22] is 0.7 Ω cm^2 with BZCY7 electrolyte thickness 10 μm.

By sweeping the cell operating points along *V–I* curve, and measuring cell impedance spectra at every single operating point,

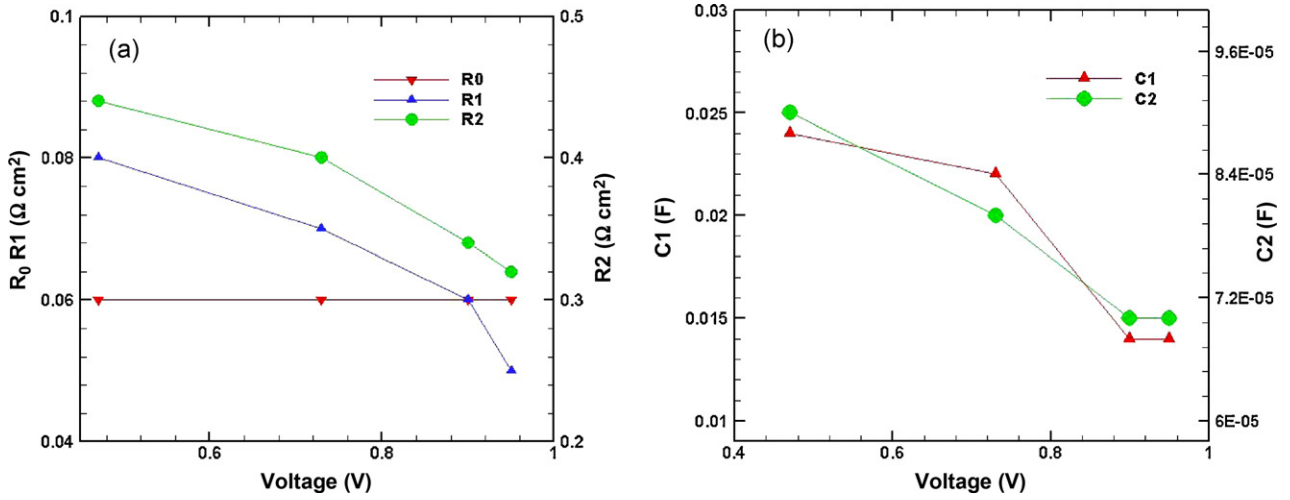

Fig. 7. (a) The polarization resistance of individual processes R_o, R_1 and R_2 through curve fitting technique and (b) capacitance value C_1 and C_2 under different voltage conditions.

we may examine the importance and role of different polarization processes under different load conditions. Fig. 6(a) shows the impedance spectra of the cell at 700 °C under different voltage conditions. The corresponding total cell resistance (R_t), ohmic resistance (R_o), as well as polarization resistance (R_p) are shown in Fig. 6(b). It is obvious to see that R_t increases from 0.433 Ω cm^2, to 0.469 Ω cm^2, 0.533 Ω cm^2, 0.581 Ω cm^2 with decreasing cell voltages from 0.95 V to 0.95 V, 0.73 V, 0.47 V, respectively. The cell loads have little effects on R_o. The R_p values increase from 0.373 Ω cm^2 to 0.409 Ω cm^2, 0.477 Ω cm^2, 0.527 Ω cm^2 with decreasing cell voltages. Decreasing the cell voltage leads to the increase of cell current and enhanced electrochemical reactions. Accordingly, the polarization resistance increases. To verify the consistence between the area specific resistance (ASR), the value obtained by calculating the slope of *I–V* curve at different voltages (Fig. 4) is compared to the value obtained from EIS (intercept at low frequency in Fig. 6(a)) at 700 °C. As shown in Fig. 6(c), we can see that the slope of *I–V* curve is consistent with cell total ASR. However, these two values cannot be perfectly matched due to system uncertainty and measurement noise.

The impedance spectra in Fig. 6(a) consist of two arcs, indicating that at least two polarization processes are involved. It is generally recognized that the high frequency arc could be attributed to charge migration processes while the low frequency arc could be attributed to mass transfer processes. In order to identify the polarization resistance of individual processes, the equivalent circuit shown in Fig. 6(a) is obtained for impedance spectra through curve fitting technique using software Z view. In the equivalent circuit, R_o is the ohmic resistance; R_1 and R_2 parallel with C_1 and C_2, representing the low frequency arc and high frequency arc, respectively, are attributed to mass transfer processes and charge migration processes. As shown in Fig. 7(a) that the cell loads have little effects on cell ohmic resistance, which is consistent with previous analysis. The polarization resistance contributed from charge migration process increases from 0.32 Ω cm^2 to 0.44 Ω cm^2 with decreasing cell voltage loads from 0.95 V to 0.47 V, respectively. The polarization resistance contributed from mass transfer process shows similar trend, increasing from 0.05 Ω cm^2 to 0.08 Ω cm^2, respectively. When cell voltage load decreases, cell current density increases. As a result, the hydrogen/oxygen consumptions increase in anode and cathode electrodes, respectively. This leads to the increase of mass transfer losses, which is consistent with the equivalent circuit analysis results. One may also notice that the polarization resistances induced by charge migration processes is much bigger than those induced by mass transfer processes. This observation is consistent with the fact that the anode and cathode electrodes are very thin in the considered button cell and mass transport losses in porous electrodes are negligible. Shown in Fig. 7(b) are the capacitance C_1 and C_2 changes with respect to the cell voltage load. Obviously, C_1 and C_2 increase when the cell voltage load decreases.

4. Conclusions

A new anode-supported SOFC material system Ni–BZCYYb/BZCYYb/PBCO was investigated. A layered perovskite oxide, $PrBaCo_2O_{5+\delta}$ (PBCO) and simple perovskite BZCYYb were synthesized and evaluated. The electrical conductivity of PBCO reached 141, 125 and 109 S cm^{-1} at 600, 650 and 700 °C, respectively. The button cell was fabricated by a simple dry-pressing/co-firing process. The performance of the button cell was tested and characterized under intermediate temperature range from 600 to 700 °C with humified H_2 (~3% H_2O) as fuel, ambient air as oxidant. The results show that the open-circuit potential of 0.983 V and maximal power density of 490 mW cm^{-2} are achieved at 700 °C. By co-doping barium zirconate–cerate with Y and Yb, the conductivity of electrolyte was significantly improved. The polarization resistances contributed from both charge migration processes and mass transfer processes increase with decreasing cell voltage loads. However the polarization resistance induced by mass transfer processes is negligible in the button cell.

Acknowledgments

This work is supported by U.S. DOE under grant no. DESC0001061 through Energy Frontier Research Center (EFRC) titled “Science Based Nanostructure Design and Synthesis of Heterogeneous Functional Materials for Energy Systems” and by U.S. DOE under contract no. DE-FG36-08GO88116 through the project titled “Hydrogen fuel cell development at Columbia, SC”.

References

[1] D.J.L. Brett, A. Atkinson, N.P. Brandon, S.J. Skinner, Chem. Soc. Rev. 37 (2008) 1568.
[2] H. Ding, X. Xue, Electrochim. Acta 55 (2010) 3812.
[3] H. Ding, X. Xue, J. Power Sources 195 (2010) 4139.
[4] A. Sammells, R. Cook, J. White, J. Osborne, R. MacDuff, Solid State Ionics 52 (1992) 111.
[5] A.K. Demin, P.E. Tsiakaras, V.A. Sobyanin, S.Yu. Hramova, Solid State Ionics 152–153 (2002) 555.
[6] C. Zuo, S. Zha, M. Liu, M. Hatano, M. Uchiyama, Adv. Mater. 18 (24) (2006) 3318.
[7] L. Yang, S. Wang, K. Blinn, M. Liu, Z. Liu, Z. Cheng, M. Liu, Science 326 (2009) 126.
[8] E.P. Murray, M.J. Sever, S.A. Barnett, Solid State Ionics 148 (2002) 27.
[9] Z. Shao, S.M. Haile, Nature 431 (2004) 170.
[10] C. Xia, W. Rauch, F. Chen, M. Liu, Solid State Ionics 149 (2002) 11.
[11] A. Maignan, C. Martin, D. Pelloquin, N. Nguyen, B. Raveau, J. Solid State Chem. 142 (1999) 247.
[12] J. Peña-Martínez, A. Tarancón, D. Marrero-López, J.C. Ruiz-Morales, P. Núñez, Fuel Cells 5 (2008) 351–359.
[13] A. Tarancón, A. Morata, G. Dezanneau, S.J. Skinner, J.A. Kilner, S. Estrade, F. Hernandez-Ramırez, F. Peiro, J.R. Morante, J. Power Sources 174 (2007) 255–263.
[14] C. Frontera, J.L. García-Muñoz, A. Llobet, L. Mañosa, M.A.G. Aranda, J. Solid State Chem. 171 (2003) 349.
[15] M. Respaud, C. Frontera, J.L. García-Muñoz, M.Á.G. Aranda, B. Raquet, J.M. Broto, H. Rakoto, M. Goiran, A. Llobet, J. Rodríguez-Carvajal, Phys. Rev. B 64 (2001) 214401.
[16] H. Ding, X. Xue, J. Alloy Compd. 496 (2010) 683.
[17] J.H. Kim, M. Cassidy, J.T.S. Irvine, J. Bae, J. Electrochem. Soc. 156 (2009) 682.
[18] K. Zhang, L. Ge, R. Ran, Z. Shao, S. Liu, Acta Mater. 56 (2008) 4876.
[19] E. Boehm, J.-M. Bassat, M.C. Steil, P. Dordor, F. Mauvy, J.-C. Grenier, Solid State Sci. 5 (2003) 973.
[20] J. Larminie, A. Dicks, Fuel Cell Systems Explained, 2nd ed., John Wiley, 2003.
[21] L. Zhao, B. He, B. Lin, H. Ding, S. Wang, Y. Ling, R. Peng, G. Meng, X. Liu, J. Power Sources 194 (2009) 835.
[22] B. Lin, S. Zhang, L. Zhang, L. Bi, H. Ding, X. Liu, J. Gao, G. Meng, J. Power Sources 177 (2009) 330.